Development of Five-Phase Multi-Mode Reluctance Motor with Current Vector Control for xEV Application

Ryo Kokubu [1] **Kyohei Kiyota** [2]

1) Electrical and Electronic Engineering, School of Engineering, Institute of Science Tokyo, Tokyo, Japan
E-mail: kokubu.r@belm.ee.titech.ac.jp
2) Electrical and Electronic Engineering, School of Engineering, Institute of Science Tokyo, Tokyo, Japan
E-mail: kiyota@ee.e.titech.ac.jp

ABSTRACT: Multi-Mode Reluctance Motor (MRM) represents an innovative technology for sustainable non-rare-earth motors. MRMs improve performance through transitions between high-efficiency SynRM and high-power SRM modes. MRMs also require only the minimal current control freedom equivalent to the number of motor phases and minimize the cost increase associated with the drive circuit. This paper discusses the theoretical derivation and potential application of current vector control for a five-phase MRM. This paper also presents case studies on torque control and design optimization of a 12-pole 20-slot 5-phase MRM for the traction motor of xEVs.

KEY WORDS: Synchronous Reluctance Motor, Switched Reluctance Motor, Multi-Mode Reluctance Motor, Current Vector Control

1. INTRODUCTION

Today, the electrification of mobility is progressing at a rapid pace. The traction motors of xEVs require high power and efficiency performance, specifically power during high-speed cruising, efficiency during urban driving, and torque during acceleration and deceleration. Interior Permanent Magnet Synchronous Motors (IPMSMs) are typically employed due to their superior and appropriate performance for xEVs. However, some reports from the rare-earth market indicate economic risks associated with the supply of magnetic material [1,2]. Fig. 1 illustrates the CNY-based market prices of two major rare-earth materials: Neodymium (Nd) Oxide and Dysprosium (Dy) Oxide. The peak prices for each occurred in February 2022 over the past 5 years, which are higher than the bottoms of each two to three times. Consequently, reducing dependence on rare-earth materials in an unstable market is crucial for the industry.

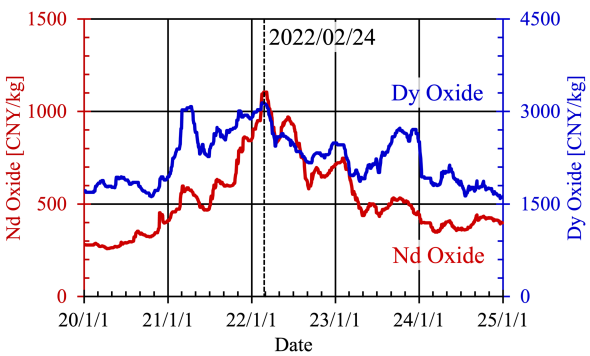

Fig. 1 Market price of Nd oxide and Dy oxide [2]

Recently, reluctance motors have attracted attention due to their low manufacturing costs as non-rare-earth motors and their high robustness to temperature fluctuations and mechanical stress [3]. This is achieved by eliminating both the permanent magnets and secondary windings, distinguishing them from IPMSMs and Induction Motors (IMs). In particular, Switched Reluctance Motors (SRMs) are capable of delivering sufficient torque and power per unit volume, comparable to those of previous IPMSMs [4]. However, iron loss increases at high speeds due to the asynchronous magnetic field compared to synchronous motors. Alternatively, Synchronous Reluctance Motors (SynRMs) offer similar advantages. The synchronous magnetic field results in low iron loss and high efficiency [5], in contrast to SRMs. However, they are less effective than SRMs in terms of power at high speeds, which is a common characteristic of synchronous motors.

The Multi-mode Reluctance Motor (MRM) represents an innovative technology for sustainable non-rare-earth motors. MRMs require only the minimal current control freedom equivalent to the number of motor phases to facilitate the transition between high-efficiency SynRM and high-power SRM modes. Therefore, MRMs minimize the cost increase associated with the drive circuit, despite the performance improvement provided by the mode transition. Additionally, a 12-pole 20-slot 5-phase MRM was proposed in [6], designed for the traction motor in 3rd-Gen Toyota Prius. This achieves higher torque and efficiency compared to a previously proposed reluctance motor in [7].

This paper discusses the theoretical derivation and potential application of current vector control in a 12-pole 20-slot 5-phase MRM. First, the mathematical formulation of current vector control is presented, along with its implementation based on the principle of MRM. Next, a case study on torque control and design optimization of MRM are introduced. Current vector control enables the maximum torque per ampere (MTPA) condition. This approach is effectively utilized in the design and control of traction motors for xEVs, ensuring the required torque is achieved under the winding and current constraints. Finally, the performance of the designed MRM is evaluated, demonstrating higher torque and efficiency compared to the previous reluctance motor.

2. Overview of MRM

2.1. Definition of structure and winding

MRMs have a doubly-salient type structure for both the stator and rotor cores with its pole numbers of stator n_s and rotor n_p. The stator core has a short-pitch concentrated winding as an individual coil in each of its slots. The polarity of adjacent coils is inverted.

Let N_s and N_p be mutually bound by the following constraints

$$N_s \in \{x \geq 3 \ \wedge \ x \equiv 1 \ (\mathrm{mod}\ 2)\} \quad (1)$$

$$N_p \in \{x \geq 3 \ \wedge \ x \equiv 1 \ (\mathrm{mod}\ 2)\} \quad (2)$$

$$\gcd(N_s, N_p) = 1 \quad (3)$$

where gcd denotes the *greatest-common-divisor*.

n_s and n_p are determined from N_s, N_p and k as follows

$$k \in \mathbb{N} \quad (4)$$

$$n_s = 2kN_s \quad (5)$$

$$n_p = 2kN_p \quad .(6)$$

In total, there are $2k$ coils, arranged N_s apart from each other and wired together per phase, regardless the number of series or parallel. Consequently, N_s-phase windings are established, where N_s is equivalent to the number of motor phase of SynRMs and SRMs. Since N_s is an odd number and greater than three, the polarity of the coils in each phase also exhibits anti-periodicity, corresponding to the periodicity of the coil arrangement.

Fig. 1 illustrates an example of a 5-phase MRM, which has $n_s = 10$ and $n_p = 6$ derived from $N_s = 5$, $N_p = 3$ and $k = 1$.

2.2. Definition of excitation phase

Fig. 2 illustrates two distinct inverter topologies for N_s-phase MRMs: half-bridged (a) and full-bridged (b) configurations. These allow the current to be either unidirectional or bidirectional.

The mechanical position of each winding determines the value of $0 \leq m_p \leq N_s - 1$, which increases by 1 in the direction of rotation, with 0 as the reference criterion. Similarly, the excitation phase of each winding determines the value of $0 \leq m_s \leq N_s - 1$,

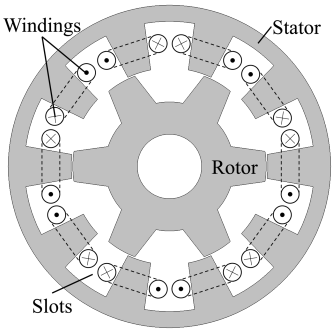

Fig. 1 An example configuration of MRM

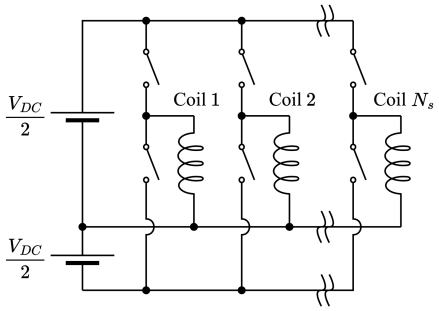

(a) Half-bridged configuration

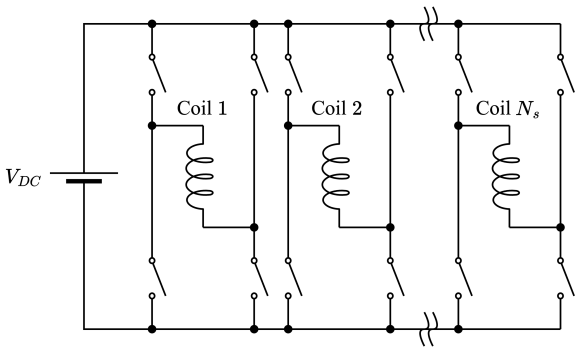

(b) Full-bridged configuration

Fig. 2 Inverter circuit topologies for MRMs

which increases by 1 in the direction of time, with 0 as the reference criterion. The correspondence between m_p and m_s is derived using N_s, N_p, k and the following equations.

In SynRM mode, the polarity of the winding current reverses each time the rotor pole aligns the stator pole, and the excitation phase is determined by

$$N_p m_p \equiv 2m_s \ (\mathrm{mod}\ N_s) \quad .(7)$$

In SRM mode, the polarity of the winding current remains unchanged regardless of the rotor's mechanical position, and the excitation phase is determined by

$$N_p m_p \equiv 1m_s \ (\mathrm{mod}\ N_s) \quad .(8)$$

3. Current Vector Control of 5-phase MRM

3.1. Basic Principle of Current Vector Control

Current vector control treats the coil current as a system state and applies a transformation matrix based on the winding arrangement and rotor position. To maintain the same current

$$\mathbf{Q}_{SynRM} = \sqrt{\frac{2}{5}}\begin{bmatrix} \cos\left(1\times 0\times\frac{2\pi}{5}\right) & \cos\left(1\times 1\times\frac{2\pi}{5}\right) & \cos\left(1\times 2\times\frac{2\pi}{5}\right) & \cos\left(1\times 3\times\frac{2\pi}{5}\right) & \cos\left(1\times 4\times\frac{2\pi}{5}\right) \\ \sin\left(1\times 0\times\frac{2\pi}{5}\right) & \sin\left(1\times 1\times\frac{2\pi}{5}\right) & \sin\left(1\times 2\times\frac{2\pi}{5}\right) & \sin\left(1\times 3\times\frac{2\pi}{5}\right) & \sin\left(1\times 4\times\frac{2\pi}{5}\right) \\ \cos\left(3\times 0\times\frac{2\pi}{5}\right) & \cos\left(3\times 1\times\frac{2\pi}{5}\right) & \cos\left(3\times 2\times\frac{2\pi}{5}\right) & \cos\left(3\times 3\times\frac{2\pi}{5}\right) & \cos\left(3\times 4\times\frac{2\pi}{5}\right) \\ \sin\left(3\times 0\times\frac{2\pi}{5}\right) & \sin\left(3\times 1\times\frac{2\pi}{5}\right) & \sin\left(3\times 2\times\frac{2\pi}{5}\right) & \sin\left(3\times 3\times\frac{2\pi}{5}\right) & \sin\left(3\times 4\times\frac{2\pi}{5}\right) \\ \sqrt{1/2} & \sqrt{1/2} & \sqrt{1/2} & \sqrt{1/2} & \sqrt{1/2} \end{bmatrix} \tag{12}$$

$$\mathbf{T}_{SynRM} = \begin{bmatrix} \cos(1\theta_e) & \sin(1\theta_e) & 0 & 0 & 0 \\ -\sin(1\theta_e) & \cos(1\theta_e) & 0 & 0 & 0 \\ 0 & 0 & \cos(3\theta_e) & \sin(3\theta_e) & 0 \\ 0 & 0 & -\sin(3\theta_e) & \cos(3\theta_e) & 0 \\ 0 & 0 & 0 & 0 & 1 \end{bmatrix} \tag{13}$$

$$\mathbf{Q}_{SRM} = \sqrt{\frac{2}{5}}\begin{bmatrix} \cos\left(2\times 0\times\frac{2\pi}{5}\right) & \cos\left(2\times 1\times\frac{2\pi}{5}\right) & \cos\left(2\times 2\times\frac{2\pi}{5}\right) & \cos\left(2\times 3\times\frac{2\pi}{5}\right) & \cos\left(2\times 4\times\frac{2\pi}{5}\right) \\ \sin\left(2\times 0\times\frac{2\pi}{5}\right) & \sin\left(2\times 1\times\frac{2\pi}{5}\right) & \sin\left(2\times 2\times\frac{2\pi}{5}\right) & \sin\left(2\times 3\times\frac{2\pi}{5}\right) & \sin\left(2\times 4\times\frac{2\pi}{5}\right) \\ \cos\left(4\times 0\times\frac{2\pi}{5}\right) & \cos\left(4\times 1\times\frac{2\pi}{5}\right) & \cos\left(4\times 2\times\frac{2\pi}{5}\right) & \cos\left(4\times 3\times\frac{2\pi}{5}\right) & \cos\left(4\times 4\times\frac{2\pi}{5}\right) \\ \sin\left(4\times 0\times\frac{2\pi}{5}\right) & \sin\left(4\times 1\times\frac{2\pi}{5}\right) & \sin\left(4\times 2\times\frac{2\pi}{5}\right) & \sin\left(4\times 3\times\frac{2\pi}{5}\right) & \sin\left(4\times 4\times\frac{2\pi}{5}\right) \\ \sqrt{1/2} & \sqrt{1/2} & \sqrt{1/2} & \sqrt{1/2} & \sqrt{1/2} \end{bmatrix} \tag{17}$$

$$\mathbf{T}_{SRM} = \begin{bmatrix} \cos(2\theta_e) & \sin(2\theta_e) & 0 & 0 & 0 \\ -\sin(2\theta_e) & \cos(2\theta_e) & 0 & 0 & 0 \\ 0 & 0 & \cos(4\theta_e) & \sin(4\theta_e) & 0 \\ 0 & 0 & -\sin(4\theta_e) & \cos(4\theta_e) & 0 \\ 0 & 0 & 0 & 0 & 1 \end{bmatrix} \tag{18}$$

RMS remains before and after transformation, the orthogonal transformation matrix $\mathbf{Q}^{5\times5}$ and the rotational transformation matrix $\mathbf{T}^{5\times5}$ must satisfy the following conditions:

$$\mathbf{QQ^{-1}} = \mathbf{E}^{5\times5} \tag{9}$$

$$\mathbf{TT^{-1}} = \mathbf{E}^{5\times5} \tag{10}$$

where **E** is the identity matrix. Additionally, the arrangement of the elements in the current state $\boldsymbol{I}_{phase}$ correspond to m_s in SynRM mode; $(m_p, m_s) = \langle(0,0),(1,4),(2,3),(3,2),(4,1)\rangle$.

$$\boldsymbol{I}_{phase} = \begin{bmatrix} i_u \\ i_v \\ i_w \\ i_x \\ i_y \end{bmatrix} \tag{11}$$

3.2. Formulations in SynRM mode

The current vector in SynRM mode, $\boldsymbol{I}_{SynRM}$, is defined and obtained by applying $\mathbf{Q}_{SynRM}$ and $\mathbf{T}_{SynRM}$, introduced in (12) and (13), to the current state $\boldsymbol{I}_{phase}$. These transformation matrices consider the 3rd harmonic component i_{d3} and i_{q3} in addition to the 1st fundamental component i_{d1} and i_{q1}.

$$\boldsymbol{I}_{SynRM} = \begin{bmatrix} i_{d1} \\ i_{q1} \\ i_{d3} \\ i_{q3} \\ i_z \end{bmatrix} = \mathbf{T}_{SynRM}\mathbf{Q}_{SynRM}\boldsymbol{I}_{phase} \tag{14}$$

$$\boldsymbol{I}_{phase} = \mathbf{Q}_{SynRM}{}^{-1}\mathbf{T}_{SynRM}{}^{-1}\boldsymbol{I}_{SynRM} \tag{15}$$

$\boldsymbol{I}_{SynRM}$ is determined by three variables α, β_1 and β_3, as well as the RMS value of coil current I_{rms}.

$$\boldsymbol{I}_{SynRM} = \begin{bmatrix} i_{d1} \\ i_{q1} \\ i_{d3} \\ i_{q3} \\ i_z \end{bmatrix} = \sqrt{5}I_{rms}\begin{bmatrix} \cos\alpha\cos\beta_1 \\ \cos\alpha\sin\beta_1 \\ \sin\alpha\cos\beta_3 \\ \sin\alpha\sin\beta_3 \\ 0 \end{bmatrix} \tag{16}$$

3.3. Formulations in SRM mode

The current vector in SRM mode, $\boldsymbol{I}_{SRM}$, is defined and obtained by applying $\mathbf{Q}_{SRM}$ and $\mathbf{T}_{SRM}$, introduced in (17) and (18), to the current state $\boldsymbol{I}_{phase}$. These transformation matrices consider 4th harmonic component i_{d4} and i_{q4} in addition to DC plus 2nd fundamental components i_z, i_{d2} and i_{q2}.

$$\boldsymbol{I}_{SRM} = \begin{bmatrix} i_{d2} \\ i_{q2} \\ i_{d4} \\ i_{q4} \\ i_z \end{bmatrix} = \mathbf{T}_{SRM}\mathbf{Q}_{SRM}\boldsymbol{I}_{phase} \tag{19}$$

$$\boldsymbol{I}_{phase} = \mathbf{Q}_{SRM}{}^{-1}\mathbf{T}_{SRM}{}^{-1}\boldsymbol{I}_{SRM} \tag{20}$$

$\boldsymbol{I}_{SRM}$ is determined by three variables γ, α, β_2 and β_4 as well as the RMS value of coil current I_{rms}.

$$\boldsymbol{I}_{SRM} = \begin{bmatrix} i_{d2} \\ i_{q2} \\ i_{d4} \\ i_{q4} \\ i_z \end{bmatrix} = \sqrt{5}I_{rms}\begin{bmatrix} \sin\gamma\cos\alpha\cos\beta_2 \\ \sin\gamma\cos\alpha\sin\beta_2 \\ \sin\gamma\sin\alpha\cos\beta_4 \\ \sin\gamma\sin\alpha\sin\beta_4 \\ \cos\gamma \end{bmatrix} \tag{21}$$

4. Design Optimization and Performance Analysis of 12-pole 20-slot 5-phase MRM

4.1. Design Optimization

A single-objective genetic algorithm (SO-GA) with two-dimensional finite element analysis (2-D FEA) is employed to design a 12-pole 20-slot 5-phase MRM. This paper presents a case study on design optimization, which result was published in [6] . The objective function is to maximize the maximum torque at extremely low speeds under the maximum current density in SynRM mode. Table 1 shows the design constraints determined in [6], which remain the same or equivalent to those of the previous reluctance motor in [7]. In particular, the maximum current RMS must be converted to maintain a constant total power capacity of the inverter. The optimization also considers variables that define the coil current waveforms in 5-phase current vector control, as introduced for SynRM mode in (16) and for SRM mode in (21), along with other design parameters affecting the stator and rotor structure, slot area, and the number of coil turns.

The previous reluctance motor in [7] had a maximum average torque of approximately 260 Nm at extremely low speeds. As initially introduced in [6], the SynRM mode is the preferred choice to meet the required torque. Table 3 presents the design specifications of the MRM and Fig. 3 illustrates its design drawing. Unlike typical SRMs, there is a little difference between the stator tooth width 8.8º and the rotor tooth width 10.0º.

Fig. 4 displays the winding arrangement, excitation phase and approximate magnetic flux density distribution for each mode in the designed MRM. In the SynRM mode in Fig. 4(a), the rotor excitation direction remains constant. The symbols U, V, W, X and Y correspond to the current vector control definition in the SynRM mode, following the same order of m_s given in (7). In contrast, in the SRM mode in Fig. 4(b), the stator excitation direction remains constant. The symbols do not correspond to the order of m_s given in (8), as the transformation matrix switches from SynRM mode (12) to SRM mode (17) without modifying the winding arrangement shown in Fig. 7(a). The excitation order is U, X, V, Y and W, which is the same of m_s given in (8).

4.2. Torque vs. Efficiency and Losses at 7500 r/min

Fig. 5 presents the driving range, efficiency, and corresponding losses for each mode at 7500 r/min. The SynRM mode maintains consistently high efficiency compared to the SRM mode, reaching a peak efficiency of 96.4 %. In the coexistence region, torque and copper losses are nearly identical for both modes. However, iron losses remain consistently lower in the SynRM mode due to reduced rotor flux fluctuations. Conversely, the SRM mode

Table 1 Design constraints

Parameter	Value	Unit
Number of Motor Phase	5	-
Number of Pole	12	-
Number of Slot	20	-
Stack Length	87	mm
Stator Diameter	264	mm
Steel Lamination	35A300	-
Space Factor of Steel Lamination	97	%
Air Gap Length	0.5	mm
Maximum Speed	13900	r/min
DC Link Voltage	650	V
Type of Inverter Unit	Full-Bridge	-
Number of Inverter Phase	5	-
Series /Parallel of Coil per Phase	4 / 1	-
Maximum Current Density	24.1	A/mm^2
Maximum Current RMS	82.8	Arms
Space Factor of Coil per Slot	54	%

Table 2 Design specifications

Parameter	Value	Unit
Rotor Diameter	184	mm
Number of Coil Turns	36	-
Winding Resistance	0.224	Ω
Maximum Torque	284.7	Nm
Maximum Torque per Unit Volume	46.59	Nm / L
Maximum Power	123.2	kW
Maximum Power per Unit Volume	20.15	kW / L
Applied variables for 5-phase Current Vector Control	$\alpha = 19$ $\beta_1 = 53$ $\beta_3 = 153$	Deg(º)

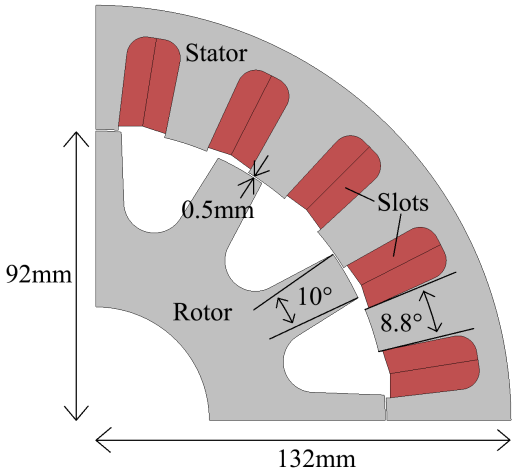

Fig. 3 Design drawing

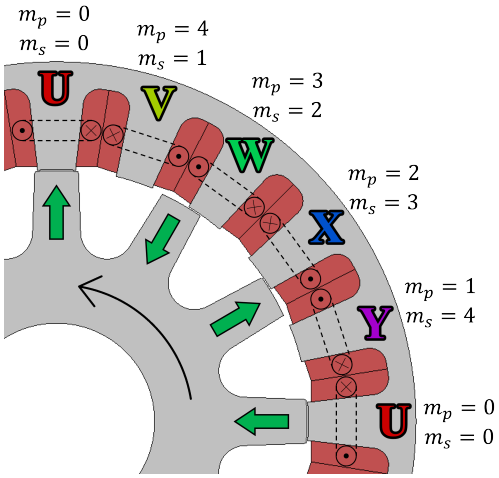

(a) SynRM mode

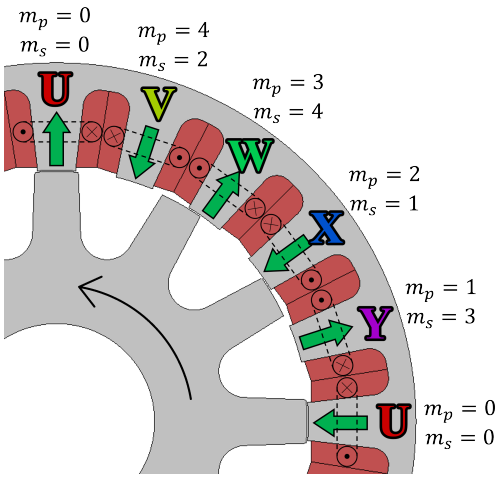

(b) SRM mode

Fig. 4 Winding arrangement and excitation order

produces higher torque than the SynRM mode, achieving a maximum torque of 132.0 Nm. This can be attributed to the continuous conduction mode, which allows coil current to flow continuously and ensure high torque at high speeds.

4.3. Speed vs Torque and Power

Fig. 6 illustrates the torque and power characteristics across the entire speed range. In SRM mode, the power increases with speed and reaches a peak of 123.2 kW at the maximum design speed of 13900 r/min, exceeding that of the previous reluctance motor[7]. Meanwhile, in SynRM mode, the maximum torque reaches 284.7 Nm at low speeds, also exceeding that of the previous reluctance motor. However, at speeds exceedingly approximately 4500 r/min, SRM mode outperforms SynRM mode in terms of maximum torque at each speed. As discussed in [6], the designed MRM exhibits lower power at medium speeds compared to the previous reluctance motor. This limitation is likely attributed to the thinner stator yoke and the increased magnetic saturation effect.

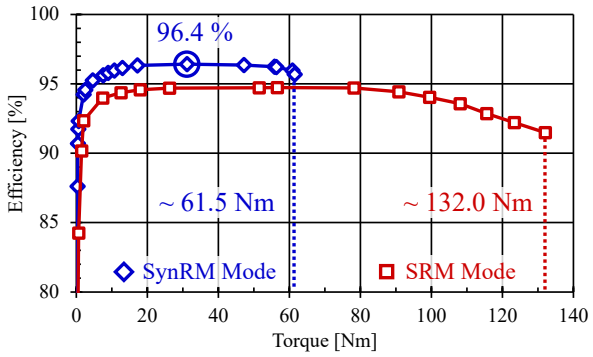

(a) Torque vs Efficiency

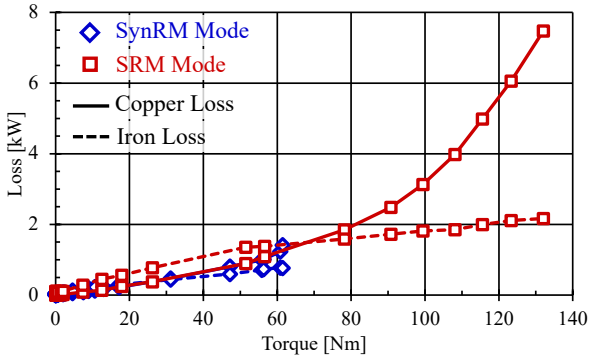

(b) Torque vs Losses

Fig. 5 Torque dependent characteristics at 7500 r/min

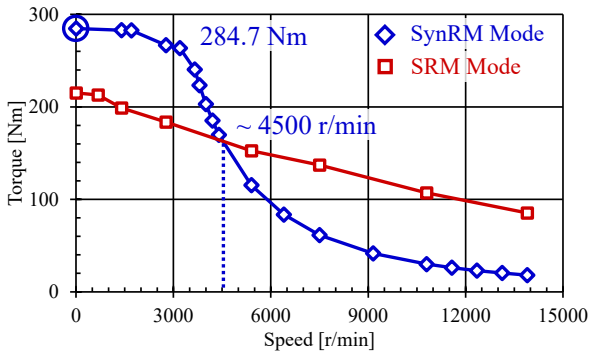

(a) Speed vs Torque

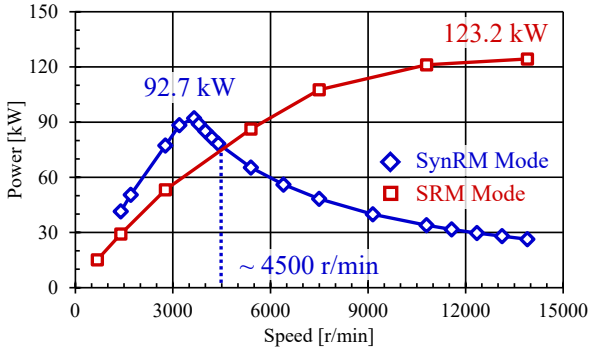

(b) Speed vs Power

Fig. 6 Speed dependent characteristics

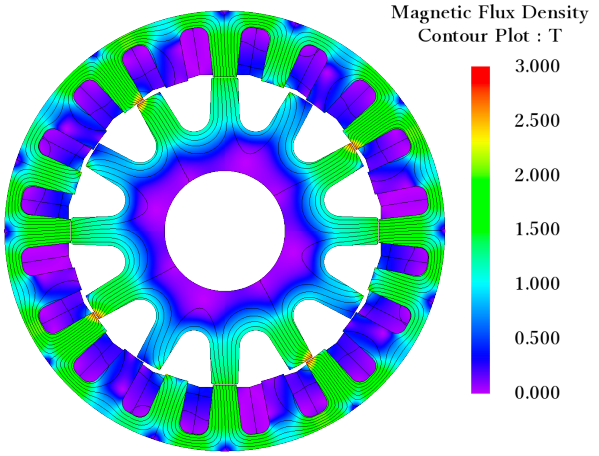

(a) Magnetic flux density distribution

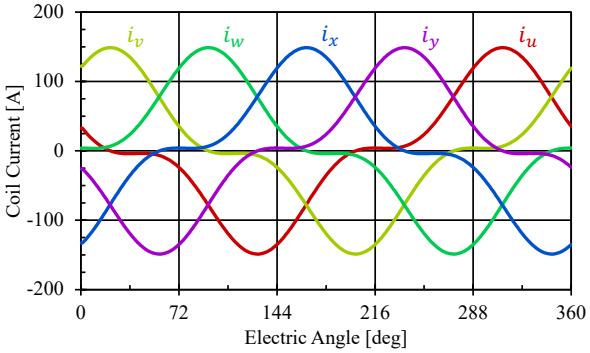

(b) Coil current waveforms

Fig. 7 Maximum torque drive in SynRM mode at low speeds

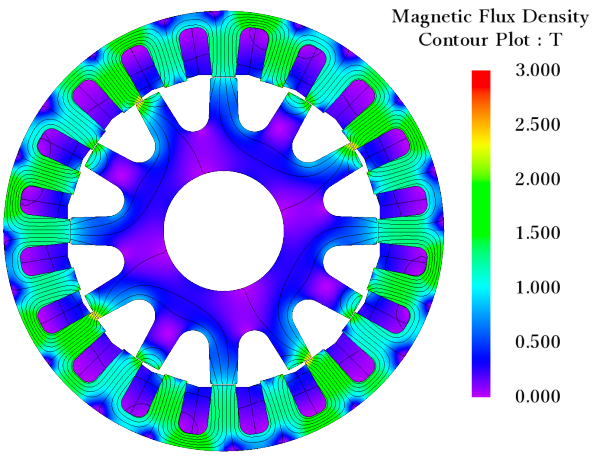

(a) Magnetic flux density distribution

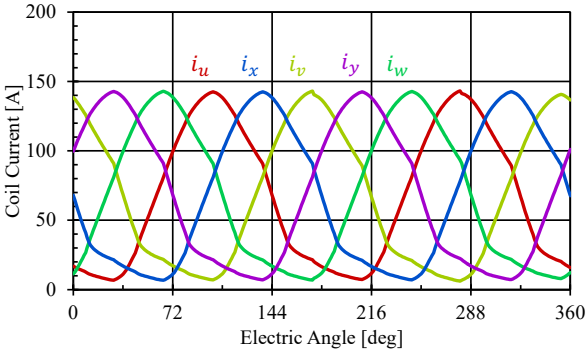

(b) Coil current waveforms

Fig. 8 Maximum power drive in SRM mode at 13900 r/min

Fig. 7 and Fig. 8 illustrate the analysis result at maximum torque drive in SynRM mode and maximum power drive in SRM mode.

The former situation is equivalent to the analysis setting on design optimization and applies 5-phase current vector control under the MTPA condition. The magnetic flux flow shown in Fig. 7(a) is similar to that illustrated in Fig. 4(a). The coil current waveforms displayed in Fig. 7(b) include not only 1st fundamental components but also 3rd harmonic components, aligning with the variable settings used in the design optimization. The best current angle under the MTPA condition for SynRM is well known as 45º even in 5-phase SynRM [8, 9]. Additionally, the method of superimposing the 3rd harmonic component onto the 1st fundamental component, known as the third harmonic current injection method, has been verified to enhance torque under the same current RMS in 5-phase SynRMs [10]. The current angle of the 1st fundamental component was treated as 45º in each case, and the 3rd harmonic component reduces the peak of the coil current waveforms. However, in this case study, β_1 reaches 53º in the SynRM-type, which is larger than previous values, and the peak of the coil current waveforms is rather increased. These findings highlight the distinct characteristics of the 5-phase MRM in SynRM mode compared to conventional SynRMs.

The latter situation is an example of applying the continuous conduction mode at high speeds in SRM mode. The magnetic flux flow shown in Fig. 8(a) is similar to that illustrated in Fig. 4(b). The coil current waveforms displayed in Fig. 7(b) have large offset and do not instantaneously drop to be 0. Although the oscillation of the flux linkage decreases with increasing speed, the power is maintained by raising the current amplitude.

This paper does not introduce the application of 5-phase current vector control to 5-phase SRM. In general, the best current angle under the MTPA condition for 3-phase SRM is derived from the relationship between i_z and i_{q2} [11], indicating that γ and β_2 should be 45º and 90º. However, literature on current vector control for 5-phase SRMs is significantly lacking.

4.4. Speed and Torque vs. Efficiency in SynRM mode

Due to the high back EMFs at high speeds, flux oriented control is implemented using a voltage source rather than current vector control. In this paper, the configuration shown in Fig. 2(b) is employed for the drive circuit, allowing the winding voltage to be

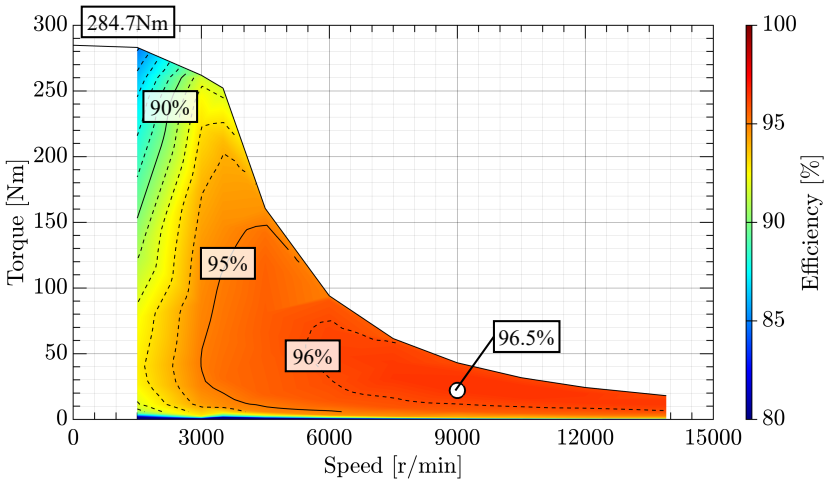

(a) Speed vs Torque

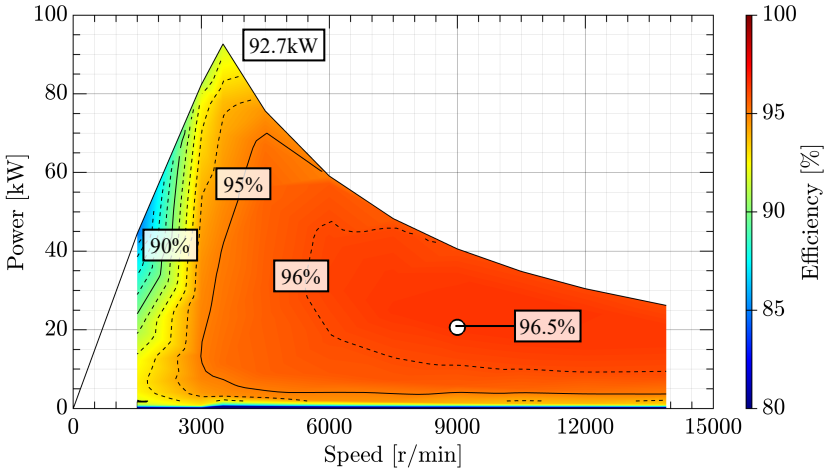

(b) Speed vs Power

Fig. 9 Efficiency map in SynRM mode

instantaneously controlled by +Vdc, 0, and -Vdc. Consequently, efficiency can be improved by incorporating a free-wheeling region using a zero-voltage loop [12] between the turn-on and turn-off phases of excitation. Notably, the previous paper [6] does not utilize the free-wheeling region and zero-voltage loop, resulting in lower efficiency compared to this paper.

Fig. 9 presents the efficiency map of the designed MRM in SynRM mode. There are regions where the efficiency achieves 95% at higher than 3000 r/min and 96% at higher than 6000 r/min. The highest efficiency reaches 96.5% around 9000 r/min. Furthermore, the efficiency at high speeds outperforms that of the previous reluctance motor [7] across all overlapping regions. In contrast, efficiency in the low-speed range remains relatively unchanged, as the torque increase compensates for the rise in copper losses associated with the greater number of coil turns. The strategy of maximizing the maximum torque at low speeds does not provide much of an improvement on efficiency at low speeds.

5. CONCLUSIONS

This paper discusses the theoretical derivation and potential application of current vector control in a 12-pole 20-slot 5-phase MRM. First, the mathematical formulation of current vector control is presented, along with its implementation based on the principle of MRM. The system state corresponding to the winding arrangement and the transformation matrices for the SynRM and SRM modes are derived. Next, a case study on torque control and design optimization of the MRM is introduced. The maximization of maximum torque at extremely low speeds under maximum current density is carried out. The best parameters of 5-phase current vector control given by the design optimization highlight the distinct characteristics of the 5-phase MRM in SynRM mode compared to conventional SynRMs. Finally, the performance of the designed MRM is evaluated, demonstrating higher torque and efficiency compared to the previous reluctance motor. There are regions where the efficiency achieves 95% at higher than 3000

r/min and 96% at higher than 6000 r/min. The highest efficiency reaches 96.5% around 9000 r/min. Furthermore, the efficiency at high speeds outperforms that of the previous reluctance motor across all overlapping regions.

Future work will include a detailed efficiency evaluation of SRM mode and testing of an actual machine. Additionally, the design methodology will be further refined by reviewing objective functions and constraints to optimize overall performance.

ACKNOWLEDGMENT

This work was supported by JST SPRING, Grant Number JPMJSP2180.

Thanks for the software license and great technical supports of JSOL CORPORATION and the great research support for rare-earth market of NeoMag Co., Ltd.

REFERENCES

[1] H. Tahanian, M. Aliahmadi and J. Faiz, "Ferrite Permanent Magnets in Electrical Machines: Opportunities and Challenges of a Non-Rare-Earth Alternative," in IEEE Transactions on Magnetics, vol. 56, no. 3, pp. 1-20, March 2020, Art no. 900120, doi: 10.1109/TMAG.2019.2957468.

[2] NeoMag Co., Ltd., https://www.neomag.jp/mag_navi/statistics/rare_earth_china.html, 2025.03.21

[3] I. Boldea, L. N. Tutelea, L. Parsa and D. Dorrell, "Automotive Electric Propulsion Systems With Reduced or No Permanent Magnets: An Overview," in IEEE Transactions on Industrial Electronics, vol. 61, no. 10, pp. 5696-5711, Oct. 2014, doi: 10.1109/TIE.2014.2301754.

[4] K. Kiyota and A. Chiba, "Design of Switched Reluctance Motor Competitive to 60-kW IPMSM in Third-Generation Hybrid Electric Vehicle," in IEEE Transactions on Industry Applications, vol. 48, no. 6, pp. 2303-2309, Nov.-Dec. 2012, doi: 10.1109/TIA.2012.2227091.

[5] M. Murataliyev, M. Degano, M. Di Nardo, N. Bianchi and C. Gerada, "Synchronous Reluctance Machines: A Comprehensive Review and Technology Comparison," in Proceedings of the IEEE, vol. 110, no. 3, pp. 382-399, March 2022, doi: 10.1109/JPROC.2022.3145662.

[6] R. Kokubu and K. Kiyota, "Proposal of 12-Pole 20-Slot Five-Phase Multi-mode Reluctance Motor," 2024 IEEE Energy Conversion Congress and Exposition (ECCE), Phoenix, AZ, USA, 2024, pp. 5742-5749, doi: 10.1109/ECCE55643.2024.10861832.

[7] K. Kiyota, K. Ichiyanagi, K. Amei and T. Ohji, "Principle of a Novel Dual-mode Reluctance Motor for Electric Vehicle Applications," *2019 IEEE International Electric Machines & Drives Conference (IEMDC)*, San Diego, CA, USA, 2019, pp. 2120-2125, doi: 10.1109/IEMDC.2019.8785207.

[8] P. R. Ghosh, A. Das and G. Bhuvaneswari, "Performance comparison of different vector control approaches for a synchronous reluctance motor drive," 2017 6th International Conference on Computer Applications In Electrical Engineering-Recent Advances (CERA), Roorkee, India, 2017, pp. 320-325, doi: 10.1109/CERA.2017.8343348.

[9] S. M. Ismaeel, S. M. Allam and E. M. Rashad, "Current Vector Control Techniques of Five-Phase Synchronous Reluctance Motor Drive Systems," 2019 21st International Middle East Power Systems Conference (MEPCON), Cairo, Egypt, 2019, pp. 1180-1185, doi: 10.1109/MEPCON47431.2019.9007981.

[10] Ruhe Shi, H. A. Toliyat and A. El-Antably, "Field oriented control of five-phase synchronous reluctance motor drive with flexible 3/sup rd/ harmonic current injection for high specific torque," Conference Record of the 2001 IEEE Industry Applications Conference. 36th IAS Annual Meeting (Cat. No.01CH37248), Chicago, IL, USA, 2001, pp. 2097-2103 vol.3, doi: 10.1109/IAS.2001.955915.

[11] N. Nakao and K. Akatsu, "Vector control specialized for switched reluctance motor drives," 2014 International Conference on Electrical Machines (ICEM), Berlin, Germany, 2014, pp. 943-949, doi: 10.1109/ICELMACH.2014.6960294.

[12] W. U. N. Fernando and M. Barnes, "Electromagnetic Energy Conversion Efficiency Enhancement of Switched Reluctance Motors With Zero-Voltage Loop Current Commutation," in IEEE Transactions on Energy Conversion, vol. 28, no. 3, pp. 482-492, Sept. 2013, doi: 10.1109/TEC.2013.2272638.